2021 IEEE 18th International Symposium on Biomedical Imaging (ISBI)
April 13-16, 2021, Nice, France

2021 IEEE 18th International Symposium on Biomedical Imaging (ISBI) | 978-1-6654-1246-9/20/$31.00 ©2021 IEEE | DOI: 10.1109/ISBI48211.2021.9433923

A DEEP NEURAL NETWORK TO RECOVER MISSING DATA IN SMALL ANIMAL PET IMAGING: COMPARISON BETWEEN SINOGRAM- AND IMAGE-DOMAIN IMPLEMENTATIONS

Mahsa Amirrashedi[1,2], Saeed Sarkar[1,2], Hossein Ghadiri[1,2], Pardis Ghafarian[3,4], Habib Zaidi[5,6,7,8], Mohammad Reza Ay[1,2]

[1]Department of Medical Physics and Biomedical Engineering, Tehran University of Medical Sciences, Tehran, Iran

[2]Research Center for Molecular and Cellular Imaging, Tehran University of Medical Sciences, Tehran, Iran

[3]Chronic Respiratory Diseases Research Center, National Research Institute of Tuberculosis and Lung Diseases (NRITLD), Shahid Beheshti University of Medical Sciences, Tehran, Iran

[4]PET/CT and Cyclotron Center, Masih Daneshvari Hospital, Shahid Beheshti University of Medical Sciences, Tehran, Iran

[5]Division of Nuclear Medicine and Molecular Imaging, Geneva University Hospital, Geneva CH-1211, Switzerland

[6]Geneva University Neurocenter, Geneva University, CH-1205 Geneva, Switzerland

[7]Department of Nuclear Medicine and Molecular Imaging, University of Groningen, University Medical Center Groningen, 9700 RB Groningen, Netherlands

[8]Department of Nuclear Medicine, University of Southern Denmark, 500 Odense, Denmark

ABSTRACT

Missing areas in PET sinograms and severe image artifacts as a consequence thereof, still gain prominence not only in sparse-ring detector configurations but also in full-ring PET scanners in case of faulty detectors. Empty bins in the projection domain, caused by inter-block gap regions or any failure in the detector blocks may lead to unacceptable image distortions and inaccuracies in quantitative analysis. Deep neural networks have recently attracted enormous attention within the imaging community and are being deployed for various applications, including handling impaired sinograms and removing the streaking artifacts generated by incomplete projection views. Despite the promising results in sparse-view CT reconstruction, the utility of deep-learning-based methods in synthesizing artifact-free PET images in the sparse-crystal setting is poorly explored. Herein, we investigated the feasibility of a modified U-Net to generate artifact-free PET scans in the presence of severe dead regions between adjacent detector blocks on a dedicated high-resolution preclinical PET scanner. The performance of the model was assessed in both projection and image-space. The visual inspection and quantitative analysis seem to indicate that the proposed method is well suited for application on partial-ring PET scanners.

Index Terms— small animal PET, deep learning, gap correction, sparse detector configuration.

1. INTRODUCTION

Owing to its enriched quantitative capability, the applications of Positron Emission Tomography (PET) have expanded drastically during the last few years. The image quality and diagnostic confidence in PET studies depend heavily upon the number of true lines of response (LORs) captured during the scanning procedure. In the pursuit of higher sensitivity and improved image quality, a new generation of total-body PET scanners with a larger axial field-of-view and hence increased number of detectors have been considered both in clinical and preclinical research settings and are beginning to reach the market [1-3]. Despite a multitude of advantages, increasing the number of detector modules comes with several issues, the most common being is the increased design complexity and higher instrumentation/service cost particularly in the case of *so-*

called bad detectors. Any deficiency in the detector modules appears as diagonal bins with zero counts in the sinogram, which ultimately deteriorates the quality of the reconstructed image [4, 5]. This problem is more pronounced in scanners with a limited number of detectors, such as small-bore devices dedicated for laboratory animal imaging, organ-specific PET imagers (brain, breast, and prostate imaging systems) with open/partial ring geometry, or novel prototype models with spacing blocks. Inter-block dead space, known as gap regions, generates a crisscross shape on sinograms resulting in low-quality PET images. Heretofore, various methods have been proposed to infer the unknown projection bins or to recover corrupted images. These include interpolation, model-based strategies [6], statistical reconstruction frameworks [7], dictionary learning [8], and other traditional techniques [9]. However, comparative studies both in image-space and projection-space demonstrated that the success of these algorithms is initially determined by the amount of missing data and the selection of the related parameters [10]. Although the majority of these methods perform well for small gap areas, most of them fail to recover artifact-free images at higher levels of sparsity [10]. Recently, deep neural networks have shown great promise in mitigating streak artifacts in sparse view computed tomography (CT) [11]. Nevertheless, it is becoming clear that, with few exceptions [12], there is a lack of research investigating the potential of deep learning (DL)-enabled artifact removal in sparse-ring PET configurations. Hence, in this work, we seek to address image quality degradation via an adopted U-Net framework in a preclinical PET scanner by modeling relatively large gaps with inactive detectors. Moreover, we assessed the performance of the proposed method for both projection-space and image-space implementation.

2. MATERIAL AND METHODS

2.1. Data acquisition

The data used in this work include 30 mice (30±10gr) PET scans acquired retrospectively using the small animal Xtrim PET scanner [13]. One hour prior to imaging, each animal was administered with an average activity of 300±50 μCi of ^{18}F-FDG and scanned for 10 minutes under anesthesia. Full-view sinograms were corrected for the delay, normalization [14], decay, out of field scatter (tail-fitting), and attenuation (using two-tissue class segmentation strategy). To mimic partially-sampled sinograms, the full-view sinograms were masked with a large gap pattern which was simulated by virtually setting the counts of two edge elements in each detector block to zero. For undersampled sinograms, the effect of gap was also modeled in the system matrix, and the reconstruction was performed using the OSEM algorithm with 5 iterations and 8 subsets. The resulting whole-body images consisted of 260 × 260 × 242 volume matrices with 0.79 × 0.79 × 0.75 mm^3 voxels. Prior to training the network, images were cropped to 128 × 128 × 85 volumes to discard the background voxels and empty slices. The resulting dataset (30 scans × 85 slices/scan) was split into 2000 samples for training, 270 for the validation, and 280 as the final test for evaluating the performance of our proposed approaches. The number of training samples was enhanced by horizontal and vertical flipping. Since the gap effect is not identical all over the scanner's field-of-view (FOV), neither translation nor rotation was used for data augmentation.

2.2. U-Net architecture

Figure 1 schematically depicts the proposed U-Net model implemented through Keras and Tensorflow libraries. The model is organized into three subsections: (i) a contracting component to encode the input image by downsampling the feature map, (ii) a bottleneck section, and (iii) an expanding component to synthesize the target truth by upsampling the extracted features. Both encoder and decoder subnets consisted of three stages with two operational blocks in each stage, whereas the bottleneck section included three blocks. Each block has a batch normalization (BN) operation and a Leaky rectified linear unit (Leaky-ReLU) after each 3 × 3 convolution. Spatial down-scaling and up-scaling are accomplished using strided convolutions and the interpolation, respectively. Skip connections are integrated to concatenate the high-level features from the encoder side of the network to the decoder part. Like the first layer, the final layer is a 1 × 1 convolution for mapping the output prediction. As demonstrated in figure 2, in the image-space implementation, our network uses the advantages of residual learning in which the network struggles to learn the residual/difference image (artifacts) instead of direct mapping between input and clear images [11]. However, in the sinogram-domain implementation, we directly map the corrupted sinogram to its full-view counterpart, and then the predicted sinogram was reconstructed using the method described in section 2.1. The network was trained for 200 epochs (early stopping rule was implemented to terminate the training when validation loss was not updated after 25 epochs) to minimize the mean absolute error between network prediction and the desired output using the Adam optimizer with a non-decaying learning rate of 10^{-4}.

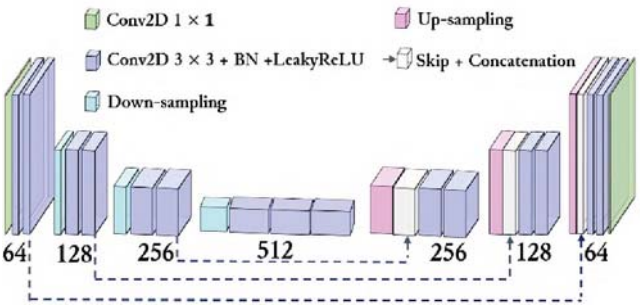

Fig. 1. The structure of our modified U-Net model.

2.3. Evaluation metrics and statistical analysis

All metrics were computed with respect to original artifact-free images, referred to as ground truth images (GI). Moreover, the relative error (RE) between AI/GI, PI/GI, and PS/GI were calculated for different organs including the brain, heart, intestine, liver as well as the whole body. For statistical analysis, paired-sample t-tests were conducted to compare the objective metrics (NRMSE, PSNR, and SSIM) between each group of AI/PI, AI/PS, and PI/PS. The difference is considered significant with a p-value < 0.05.

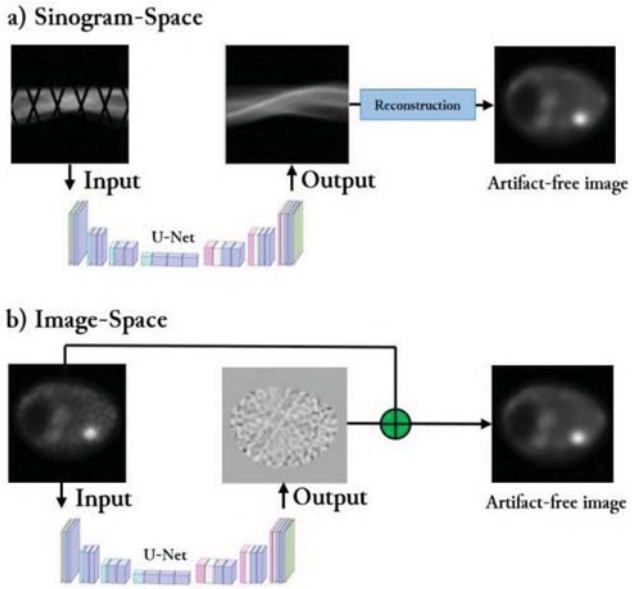

Fig. 2. Schematic diagram of sinogram-space (top) and image-space (bottom) implementations.

5. RESULTS

Figure 3 illustrates an example of artifact-corrupted unseen test dataset, artifact-free original PET, and predicted clear images in both domains along with pixel-wise relative difference images (known as SUV bias maps). Comparing to artifact-corrupted images, the predicted images in both domains demonstrated marked improvements in quality and quantitative accuracy. Besides visual inspection, this improvement is exhibited by larger PSNR/SSIM values and smaller NRMSE for corrected images, as summarized in Table 1. Regarding the statistical analysis, all metrics were improved significantly for the results predicted either in sinogram or image-space. However, these improvements are slightly more obvious for the sinogram-space gap correction. However, no significant difference was found between the PI and PS. From Figure 4, our proposed method in both domains leads to a relative SUV error of less than 5% in almost all body sections.

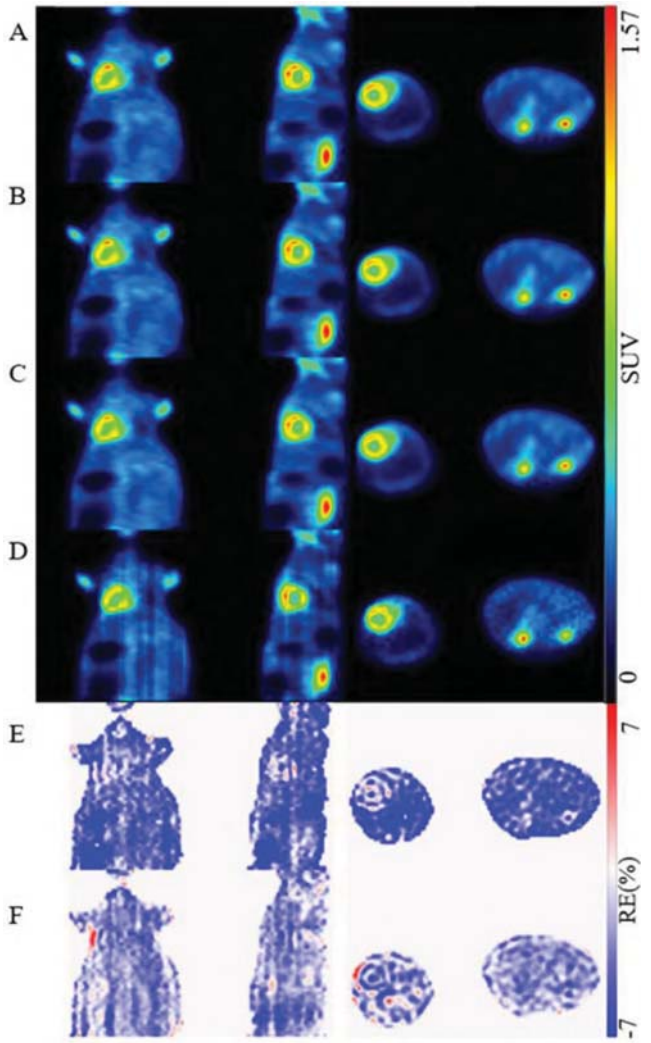

Fig. 3. Representative images from unseen test data. From left to right: Coronal, sagittal, transverse view from heart, and transverse view from kidneys. (A) Ground truth, (B) Image-domain prediction, (C) Sinogram-domain prediction, (D) artifact-corrupted image, (E) Bias maps for B, and (F) for C.

Table 1. Image quality metrics for the test dataset.

Dataset	NRMSE	PSNR	SSIM
AI	0.12±0.03	37.98±4	0.93±0.03
PS	0.051± 0.01	45.87±5	0.98±0.01
PI	0.054±0.009	44.83±5.1	0.97±0.01
P-value(AI/PS)	0.0022*	0.003*	0.0226*
P-value (AI/PI)	0.0012*	0.0019*	0.0225*
P-value (PI/PS)	0.1081	0.0824	0.0694

6. DISCUSSION AND CONCLUSION

While most gap correction strategies were implemented in the projection domain, we sought out to study the feasibility of a DL-based approach in mitigating high-frequency artifacts caused by under-sampled projections in

preclinical ^{18}F-FDG PET images and compared the outcomes with those of projection-based learning. Visual inspection and quantitative analysis showed that the predicted artifact-free images either in the image (PI) or projection-space (PS) have superior overall image quality in contrast to the ones reconstructed from incomplete views (AI). However, projection-based learning provides quantitatively smaller error which could be attributed to relatively more information in the sinogram mode presentation [15]. The disadvantage is that projection domain learning is computationally more demanding compared to image learning (~ 5 times for our study). Quantitation errors for image-based learning are more noticeable for the regions lying in the proximity of the FOV center (e.g., hallow regions with low uptake pattern in the abdomen or some small defects on the heart). In line with previous studies [12], our results proved that the DL-based scheme could be leveraged to synthesize high-quality and quantitatively accurate PET images on scanners with sparse detector configuration. However, to investigate the potential and advantages of DL-based gap correction, we plan to compare the results of our findings with those of rival methods in the future.

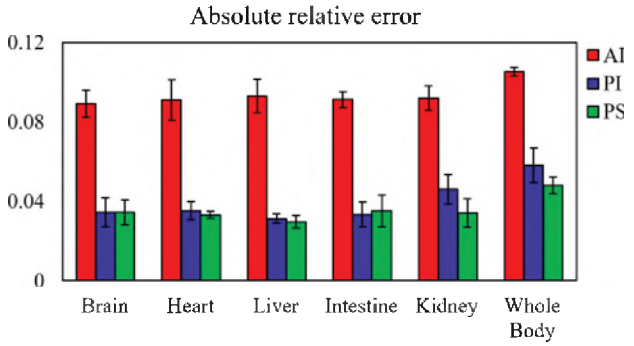

Fig. 4. Mean absolute relative error for different organs and whole-body for unseen test sets. Error bars indicate standard deviation.

7. COMPLIANCE WITH ETHICAL STANDARDS

This study was approved by Ethics committee of Tehran University of Medical Sciences. (Approval ID: IR.TUMS.MEDICINE.REC.1397.04).

8. ACKNOWLEDGMENTS

This work was supported Tehran University of Medical Sciences under grant No. 36847 and the Private Foundation of Geneva University Hospitals under Grant RC-06-01.

9. REFERENCES

[1] C. Molinos *et al.*, "Low-dose imaging in a new preclinical total-body PET/CT scanner," *Frontiers in medicine,* vol. 6, p. 88, 2019.

[2] M. Amirrashedi, H. Zaidi, and M. R. Ay, "Advances in Preclinical PET Instrumentation," *PET Clinics.*

[3] S. Vandenberghe, P. Moskal, and J. S. Karp, "State of the art in total body PET," *EJNMMI Physics,* vol. 7, pp. 1-33, 2020.

[4] W. Whiteley and J. Gregor, "CNN-based PET sinogram repair to mitigate defective block detectors," *Physics in Medicine & Biology,* vol. 64, no. 23, p. 235017, 2019.

[5] E. E. Ter Voert, G. Delso, F. de Galiza Barbosa, M. Huellner, and P. Veit-Haibach, "The effect of defective PET detectors in clinical simultaneous [18 F] FDG time-of-flight PET/MR imaging," *Molecular Imaging and Biology,* vol. 19, no. 4, pp. 626-635, 2017.

[6] U. Tuna, S. Peltonen, and U. Ruotsalainen, "Gap-filling for the high-resolution PET sinograms with a dedicated DCT-domain filter," *IEEE Transactions on Medical Imaging,* vol. 29, no. 3, pp. 830-839, 2010.

[7] P. Kinahan, J. A. Fessler, and J. Karp, "Statistical image reconstruction in PET with compensation for missing data," *IEEE transactions on Nuclear Science,* vol. 44, no. 4, pp. 1552-1557, 1997.

[8] S. Valiollahzadeh, J. W. Clark Jr, and O. Mawlawi, "Dictionary learning for data recovery in positron emission tomography," *Physics in Medicine & Biology,* vol. 60, no. 15, p. 5853, 2015.

[9] H. De Jong *et al.*, "Correction methods for missing data in sinograms of the HRRT PET scanner," in *2002 IEEE Nuclear Science Symposium Conference Record*, 2002, vol. 2, pp. 1202-1205: IEEE.

[10] S. Shojaeilangari, C. R. Schmidtlein, A. Rahmim, and M. R. Ay, "Recovery of missing data in partial geometry PET scanners: Compensation in projection space vs image space," *Medical physics,* vol. 45, no. 12, pp. 5437-5449, 2018.

[11] Y. S. Han, J. Yoo, and J. C. Ye, "Deep residual learning for compressed sensing CT reconstruction via persistent homology analysis," *arXiv preprint arXiv:1611.06391,* 2016.

[12] C. C. Liu and H. M. Huang, "Partial-ring PET image restoration using a deep learning based method.," *Phys Med Biol,* vol. 64, no. 22, p. 225014, Nov 21 2019.

[13] M. Amirrashedi *et al.*, "NEMA NU-4 2008 performance evaluation of Xtrim-PET: A prototype SiPM-based preclinical scanner," *Medical Physics,* vol. 46, no. 11, pp. 4816-4825, 2019.

[14] M. Amirrashedi, M. R. Ay, S. Sarkar, and M. H. Farahani, "Normalization of a positron emission tomography scanner ", 2020.

[15] A. Sanaat, H. Arabi, I. Mainta, V. Garibotto, and H. Zaidi, "Projection-space implementation of deep learning-guided low-dose brain PET imaging improves performance over implementation in image-space," *Journal of Nuclear Medicine,* p. jnumed. 119.239327, 2020.